AIAA-2004-1342

# Modeling Single Component Fluid Transport through Micro Channels and Free Molecule Micro-Resistojet

Reni Raju and Subrata Roy
Computational Plasma Dynamics Laboratory
Kettering University, Flint, Michigan 48504

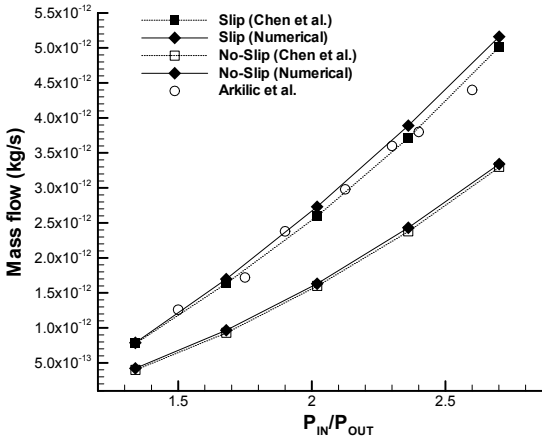


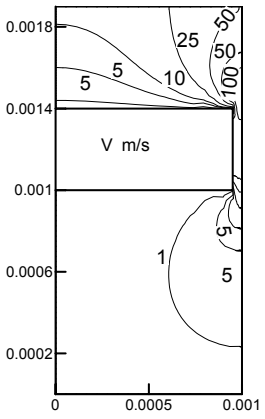


**42nd Aerospace Sciences Meeting and Exhibit**

5-8 January 2004

Reno, Nevada

# Modeling Single Component Fluid Transport through Micro Channels and Free Molecule Micro-Resistojet

**Reni Raju** [*] **and Subrata Roy** [†]
*Computational Plasma Dynamics Laboratory*
*Department of Mechanical Engineering*
*Kettering University, Flint, Michigan 48504, USA*

The study of fluid flow through tiny structures is fundamental to any future technologies. Specifically efficient numerical modeling of subsonic single component microscale flow is the subject. We implement a recently developed two-dimensional hydrodynamic finite element model for studying slip and transitional Poiseuille gas flows. The model incorporates first-order slip and temperature boundary conditions. Computed results for helium gas are compared with available experimental data for two different microchannel geometry aspect ratios. One of these cases is benchmarked with previously reported numerical solutions. Documented solutions verify that first-order slip boundary conditions yield reasonably accurate predictions within slip and transitional regime for these micro geometries. Preliminary results for argon gas flow through a free molecule micro-resistojet have also been presented.

## 1. INTRODUCTION

We shall limit our present study to low speed single component fluid flows, specifically, gas flows. Several researchers have investigated gas flow characteristics through microsystems both experimentally and numerically. Liu *et al.*[1] manufactured microsystems to measure pressure distribution along a microchannel. This was followed by studies of Pong *et al.*[2] on first and second-generation systems. Shih *et al.*[3] have extended the same to detailed measurements of both mass flow rate and pressure distribution. Arkilic *et al.* have carried out experiments for measuring the mass flow rate[4] and analyzing the tangential momentum accommodation coefficient for different gas flows.[5] Chen *et al.*[6] have studied the experimental results of Pong *et al.*[2] and Arkilic *et al.*[5] using the finite difference method with first-order slip condition.

The fluid flow through micro devices is numerically modeled using either the deterministic or statistical approach. Representative models include Navier-Stokes equations with and without wall slip,[7-10] Burnett equation (BGK model)[11], direct simulation Monte Carlo (DSMC)[12] and hybrid models. Molecular dynamics is found suitable for free-molecule flows. Computational challenges of these methods are well known.[10] Of critical importance is the fluid mean free path (mfp) described using the Chapman-Enskog result for a hard sphere gas at known temperature and viscosity. As the mfp becomes comparable to the macroscopic length scale of the physical system, the rarefaction effects become pronounced. The ratio of mfp and the representative length scale of the system is known as the Knudsen number (Kn).

For $0.001 < Kn < 0.1$, also known as the slip flow regime, Arkilic *et al.*[5] have done a two-dimensional analysis using Navier-Stokes equation with first order slip boundary conditions to study compressibility and rarefaction effects in long microchannels. Shih *et al.*[3] validated the slip model with their own data analytically. In rarefied gases having higher Kn, the conventional choice is DSMC. Karniadakis & Beskok [9] have carried out both analytical and numerical study of flow in different micro geometries using DSMC and spectral element methods.

Recently Roy *et al.*[10] have developed a finite element discretized Galerkin weak statement (GWS) based phase

[*] Graduate Research Assistant, Currently at George Washington University, reni@gwu.edu, AIAA Student member.
[†] Associate Professor, sroy@kettering.edu, AIAA Associate Fellow

space model for efficient prediction of bulk properties in slip-to-transition regime Knudsen number flows. The slip flow inside a 1.2 μm microchannel (Kn = 0.059) was compared to the reported experimental[2] and numerical[6] results while the transitional flow (Kn = 7.36) inside a 200nm diameter nanopore was validated with the experimental data. The wall transport coefficient of 20-30nm thick carbon nanotubule was determined for argon, oxygen and nitrogen.[13] Numerical results for microcolumn geometry with two 90° bends have also been reported showing the two dimensional effect of bends on small flows.[14] Similar serpentine geometry has application in many practical microfluidic devices that require longer contact length within a compact area[15,17].

This paper focuses on applying this finite element hydrodynamic model for further simulation of subsonic gaseous flow through microchannels. A detailed comparison and benchmarking of the model is done for two experimental[3,4] and one numerical data[6] published in the literature. In addition, we present the preliminary results for flow inside a free molecule micro-resistojet (FMMR). FMMR is a microthruster that operates on the principle of electrothermal propulsion where the propellant is heated electrically.[16] Principally in resistojets thermal energy is supplied to the propellant molecules due to heat transfer from an electrically heated surface as well as due to the intermolecular collisions. The thruster operates at low stagnation pressures of 50-500 Pa. The conceptual design and performance prediction for this particular type of resistojet has been reported earlier[17-19] and recently next generation designs have been presented.[20] The operating conditions of FMMR are at very low stagnation pressures (rarefied). Thus the propellant is mostly heated by the wall gas interaction with the surface maintained at an elevated temperature.

This paper is divided into following sections. Section 2 describes the geometric models for analyses. The governing equations are described in Section 3. Numerical algorithm along with imposed boundary conditions is detailed in Section 4. Section 5 documents the results and discussion. Finally, the conclusions are given in Section 6.

**NOMENCLATURE**

| | |
|---|---|
| A | Area, $m^2$ |
| $C_p$ | Specific heat at constant pressure, J/kg K |
| $g_0$ | Gravitational acceleration, $m/s^2$ |
| $\gamma$ | Specific heat ratio |
| $I_{sp}$ | Specific Impulse, s |
| k | Thermal conductivity, W/mK |
| Kn | Knudsen Number |
| $\lambda$ | Mean free path of the fluid, m |
| $m$ | Mass of gas, kg |
| $\mu$ | Coefficient of viscosity, $Ns/m^2$ |
| $P$ | Gas pressure, Pa |
| $\rho$ | Gas density, $kg/m^3$ |
| R | Gas constant, J/kg K |
| $\sigma_v$ | Tangential-momentum accommodation coefficient |
| $\sigma_T$ | Thermal accommodation coefficient |
| $\Im$ | Thrust, N |
| $t$ | Time, s |
| $T$ | Gas temperature, K |
| $u$ | Gas velocity in $x$-direction, m/s |
| $v$ | Gas velocity in $y$-direction, m/s |

Subscripts

| | |
|---|---|
| g | Gas condition |
| i | Inlet condition |
| o | Outlet condition |
| s | Expansion slot |
| w | Wall conditions |

## 2. GEOMETRIC DESCRIPTION

In this paper, three simulation cases will be analyzed with two basic geometric shapes, namely, a straight microchannel, and the FMMR geometry. The schematic of the microchannel is as shown in Figure 1. The model assumes the gas flow through two parallel plates of length $L$, width $W$ and separated by a distance $H$. Neglecting the end effects we consider only the two dimensional geometry stretching in the $x$ and $y$ directions.

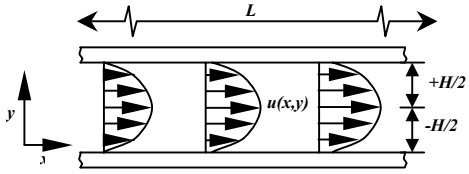


Figure 1: Schematics for Poiseuille flow inside a microchannel (*Cases I & II*).

The geometry and gas property details for microchannel flow simulation cases are listed in Table 1. Cases I and II will validate the finite element based numerical results with the experimental data of Shih *et al.*[3] and Arkilic *et al.*[4], respectively, for the different pressure ratios. Chen *et al.*[6] has reported numerical results for Case II using fine grid finite difference formulation with slip boundary conditions. The exit Kn for these two cases are 0.17 and 0.155, respectively.

Figure 2 shows the schematic of a single slot of FMMR geometry based on Ref. 17. The thruster chip is manufactured with 40 such slots of width 100 μm, length 1cm and depth 400 μm. Each slot has two 90º bends. The propellant molecules enter the FMMR chamber through the propellant inlets and the molecules undergo gas-

surface interactions in the expansion slots with the surface at the elevated temperature (heated by the heating element) gaining energy in the process.

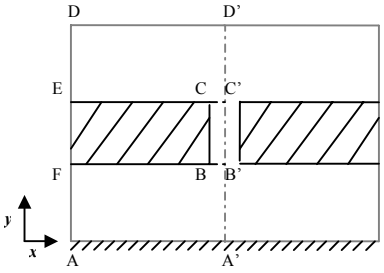


Figure 2: Schematic of the symmetric single slot inside a FMMR (***Case III***).

| Microchannel | Case I | Case II |
|---|---|---|
| Gas | Helium | Helium |
| $L$ ($\mu m$) | 4000.0 | 7500.0 |
| $W$ ($\mu m$) | 40.0 | 52.25 |
| $H$ ($\mu m$) | 1.2 | 1.33 |
| $P_i/P_o$ | 1.59,1.87, 1.92, 2.29 | 1.34, 1.68, 2.02, 2.36, 2.70 |
| $T_i$ ($K$) | 300.0 | 314.0 |
| $T_w$ ($K$) | 300.0 | 314.0 |
| **Kn** | 0.17 | 0.155 |
| $\mu$ ($Ns/m^2$) | $2.06 \times 10^{-5}$ | $2.06 \times 10^{-5}$ |
| $\gamma$ | 1.667 | 1.667 |
| **R** ($J/kg\ K$) | 2076.9 | 2076.9 |

Table 1. Microchannel dimensions and properties of fluid.

The hydrodynamic simulation of FMMR will be done on the same geometry of Ketsdever ***et al.***[17-19] for comparison purposes. The model in Figure 2 is symmetric along the slot width. The section A'D' shows the line of symmetry for the slot width. BB' and CC' are the one-half of the slot width i.e, 50 μm and represent the slot throat and slot exit respectively. AF represents the inlet through which the propellant gas molecules enter the system in the ***x***-direction with a pressure $P_i$ and temperature $T_i$. The section FBCE is the thruster chip that is maintained at a constant temperature $T_w$. The plenum temperature $T_p$ is maintained at the same temperature as the inlet $T_i$. The propellant molecules undergo gas-surface collisions with this surface and gain energy in the process when the surface is maintained at an elevated temperature. DE is again the plane of symmetry of the slot configuration. For the DSMC calculations a far field vacuum was specified at a distance of 10 slot-widths from the slot exit. However, for the hydrodynamic prediction this field was specified at a distance 5 slot widths from the exit and set to a very low exit pressure of $P_o$= 3.9 Pa. The Kn at the slot exit is 17.72 (free-molecule) for argon propellant used. The model parameters for nominal FMMR operating conditions have been listed in Table 2.

| FMMR Parameters | Case III |
|---|---|
| Gas | Argon |
| Slot width, **w** ($\mu m$) | 100 |
| Slot Thickness, **t** ($\mu m$) | 400 |
| Distance from Plenum, **d** ($\mu m$) | 1000 |
| $T_i$ ($K$) | 300 |
| $T_w$ ($K$) | 300, 600 |
| $P_i$ ($Pa$) | 50 |
| $P_o$ ($Pa$) | 3.9 |
| $R$ ($kJ/kg.K$) | 208.1 |
| $C_p$ ($k/kgK$) | 520.03 |
| $\mu$ ($N\text{-}s/m^2$) | $2.22 \times 10^{-5}$ |
| $k$ ($W/k.m$) | 0.0207 |
| $\gamma$ | 1.667 |
| Number of slots | 40 |

Table 2: FMMR model dimensions and flow conditions.

## 3. GOVERNING EQUATIONS

The following two-dimensional, compressible Navier-Stokes (NS) form with constant viscosity is used to analyze the gas flow through microchannels,

$$L(\boldsymbol{q}) = \frac{\partial \boldsymbol{q}}{\partial t} + \frac{\partial \left( \boldsymbol{f}_j - \boldsymbol{f}_j^v \right)}{\partial x_j} - s = 0 \ , 1 \le j \le 2 \tag{1a}$$

$$\boldsymbol{q} = \begin{pmatrix} \rho \\ \rho u_i \\ \rho C_p T + P \\ 0 \end{pmatrix}, \boldsymbol{f}_j = \begin{pmatrix} \rho u_j \\ u_j \rho u_i + P\delta_{ij} \\ u_j (\rho C_p T + P) \\ 0 \end{pmatrix}, \tag{1b}$$

$$\boldsymbol{f}_j^v = \begin{pmatrix} 0 \\ \tau_{ij}' \\ k\dfrac{\partial T}{\partial x_j} + \tau_{ij}' u_i \\ 0 \end{pmatrix}, s = \begin{pmatrix} 0 \\ 0 \\ 0 \\ P - \rho RT \end{pmatrix}, \quad 1 \le i \le 2$$

where $\boldsymbol{q}$ is the state variable, $\boldsymbol{f}$ is the kinetic flux vector, $\boldsymbol{f}^v$ the dissipative flux vector and $s$ is the source term; $u$ is the fluid velocity component, $\rho$ is the gas density, $T$ is the gas temperature, $t$ is the time, $P$ is the gas pressure, $R$ is the specific gas constant, and $\tau_{ij}' = \mu \left( \dfrac{\partial u_i}{\partial x_j} + \dfrac{\partial u_j}{\partial x_i} \right) + \delta_{ij} \lambda \operatorname{div} \mathbf{V}$ .

The "no-slip" wall condition in the usual continuum context is defined as having all components of the velocity vanish at the solid wall. However, as the macroscopic length scale becomes comparable to the fluid mean free path, the description becomes fuzzy and the walls "move". At this stage, streaming velocity at the wall can be described comprising of the streaming velocity of incident

particles and that of the scattered particles. The boundary condition then can be interpreted as the flux or Neumann condition from the macroscopic point of view. We derive the following first order slip relation for dilute, monatomic gas based on Maxwell[7] and Chapman-Enskog result,

$$-\mu\left(\frac{\partial u}{\partial y}\right)_w = \frac{5\rho\sigma_V\sqrt{2\pi RT}}{16\left(2-\sigma_V\right)}\left(u_{wall}-u_{gas}\right) \tag{2a}$$

The corresponding temperature-jump relation based on von Smoluchowski[8] is

$$-k\left(\frac{\partial T}{\partial y}\right)_w = \frac{\sigma_T\rho}{2-\sigma_T} f\left(T_{wall}-T_{gas}\right) \tag{2b}$$

$$\text{where}\quad f = \left[\frac{\gamma+1}{2\gamma}\right]\frac{5C_p\sqrt{2\pi RT}}{16}$$

In equations (2a-b), $u_{gas}$ and $T_{gas}$ are the velocity and temperature of the gas adjacent to the wall, while $u_{wall}$ and $T_{wall}$ are the wall velocity and wall temperature, respectively. Also the streamwise temperature gradient of the fluid (thermal creep) is neglected near the wall. The tangential-momentum accommodation coefficient, $\sigma_V$ and the thermal accommodation coefficient, $\sigma_T$ at the walls indicate the molecular fraction reflected diffusively from the walls. Based on the experimental data, Arkilic *et al.*[6] have analytically determined that for nitrogen, argon or carbon dioxide in a silicon micromachined channel the value of $\sigma_V$ ranges between 0.75-0.85.

Traditionally, the first order equations (2a-b) are applied as long as Kn < 0.1. Karniadakis & Beskok[9] have presented a higher order slip boundary condition, which is second order accurate, for predicting flow accurately for higher Knudsen number. It has been suggested that Maxwell's first order boundary condition breaks down near Kn = 0.15.[21] However, Roy *et al.*[10] and Cooper *et al.*[13] have successfully utilized the first-order hydrodynamic boundary condition to predict the gaseous flow through the micro- and nano-geometries for high Kn reaching well into the transition regime. Thus for computational efficiency, we would restrict slip to first order conditions (2a-b) for all three case studies with exit Kn ≤ 17.72.

## 4. NUMERICAL METHOD

The difficulty involved in achieving a steady state solution of equation (1a-b) directly is due to the selection of initial conditions. The conventional method of achieving a steady state solution is to use the time term as a relaxation parameter in the equation system and run the problem till all the transient features die down. Here we utilize artificial diffusion based initial condition generator.

Using any admissible test function $w$[22], the variational integral yields the *weak statement* for equation (1). Thereafter, the domain $\Omega$ and integrated variables $\boldsymbol{q}$ are spatially discretized to $\Omega_e$ and $\mathbf{Q}$ using Lagrange basis functions $N_k$ up to the degree $k$. Thus for steady state,

$$WS = \int_\Omega wL(\boldsymbol{q})\,d\Omega = 0,$$
$$\Rightarrow\ WS^h = S_e\left(\int_{\Omega_e} N_k L_e(\mathbf{Q})\,d\tau\right) \equiv 0 \tag{3a}$$

$$WS^h = S_e\left(\begin{array}{l}\int_{\Omega_e} N_k(-s)\,d\tau - \int_{\Omega_e}\frac{\partial N_k}{\partial x_j}\left(\boldsymbol{f}_j-\boldsymbol{f}_j^v\right)_e d\tau \\ +\oint_{\partial\Omega_e\cap\partial\Omega^h} N_k\left(\boldsymbol{f}_j-\boldsymbol{f}_j^v\right)_e \hat{n}_j\,d\sigma\end{array}\right) \tag{3b}$$

The superscript $h$ denotes discretisation. $S_e$ symbolizes the "assembly operator" carrying local (element $e$) matrix coefficients into the global arrays. The weak statement naturally yields the surface integrals via application of Green-Gauss theorem in equation (3b), which contains the unknown boundary fluxes wherever Dirichlet (fixed) boundary conditions are enforced. The zero gradient boundary conditions are automatically enforced via removal of the surface integral. For the slip flow boundary, appropriate surface integrals are replaced by incorporating the equations (2a-b) into the momentum and energy equations. The terminal ODE is usually solved using a Newton-Raphson scheme. The iteration ($i$) convergence of a solution vector $\mathbf{Q}$ on node $j$ is defined by the norm: $\|\mathbf{Q}_j^i - \mathbf{Q}_j^{i-1}\| \Big/ \|\mathbf{Q}_j^i\| \le \in$. We chose $\in=10^{-4}$.

The computational geometry for all cases is discretized using two-dimensional 9-noded biquadratic finite elements. The continuity and equation of state are solved for density and pressure respectively using the four corner nodes of the element. However, all nine nodes are used for velocity and temperature calculations.

Table 1 summarizes the fixed boundary conditions for Cases I and II. The gas temperature $T_i$ is specified at the inlet and based on the assumption of isothermal wall, the wall temperature $T_w$ is specified. At the inlet the velocity flux is $\partial u/\partial x$=0 and the y-component of the velocity is $v$ = 0. The pressure at the outlet, $P_0$ is 100.8 kPa for both the cases and the inlet pressure, $P_i$ is specified based on the corresponding pressure ratio. The microchannel is benchmarked using both no-slip and first order slip conditions. Shih *et al.*[3] have given the effective tangential accommodation coefficient for Case I to be 1.162. For the remaining cases since the roughness of the channel is not known, we assume the wall-gas interaction as diffusive reflection with $\sigma_V = \sigma_T \approx 1.0$ in accordance with the

reported numerical result of Chen *et al.*[6]. This is applicable to most of the engineering systems, implying that the channel surface is rough.

Table 2 describes the boundary condition for FMMR (Case III). Here the flow takes place from the inlet AF to the outlet DD' as shown in Figure 2. Inlet pressure ($P_i$) and temperature ($T_i$) are specified at AF. Plenum temperature ($T_p$) is maintained equal to inlet temperature. The outlet pressure ($P_o$) is specified at DD'. At the line of symmetries A'D' the u-component of velocity is set to be zero. On faces FB,BC and CE the wall temperature is set to be equal to $T_w$. First order slip and temperature jump boundary conditions are set at the plenum surface AA' and walls F-B-C-E with the exception of face BC which is kept as an isothermal wall with temperature $T_w$. As the flow becomes transitional, standard hydrodynamic model assumptions will run into difficulties due to incorrect modeling of the shear stress and non-equilibrium processes. Among other things, one would expect the surfaces of the transport media to play a dominant role in determining flow characteristics. In such a case one may significantly alter predicted flow properties by controlling the nature of the pore surfaces[10,13] and possibly by modifying the bulk viscosity with inclusion of the hydrodynamic quantum effect. Here, as in our prior work,[10,13] only the surface properties are used as control parameters.

## 5. RESULTS AND DISCUSSION

In this section numerical results for three cases mentioned in Sections 1 and 2 are discussed.

**Case I** is based on the experiment of Shih *et al.*[3]. The channel is 4000 μm long and 1.2 μm high with an aspect ratio of 3333. The working fluid in this case is Helium with an outlet Knudsen number of 0.17 at atmospheric conditions indicating low transitional flow. The computational geometry is discretized using 560 two-dimensional 9-noded non-overlapping bi-quadratic finite elements consisting of 2337 nodes.

For four different pressure ratios, the experimental measurements of the pressure distribution show a nonlinear trend, which are closely (within ~2%) matched by the numerical slip data as plotted in Figure 3(a). The pressure drop occurs to overcome the shear stresses in the channel. With a slip boundary the flow encounters lesser frictional forces on the wall than no-slip boundary, which tends to make the slip flow more linear as compared to the no-slip flow.

For negligible temperature change, the density variation is proportional to the pressure drop. Due to mass flux conservation, velocity increases as the density and pressure drop; however the values remain considerably low indicating a sub-sonic flow, Figure 3(b). The slip flow yields a higher velocity than the corresponding no-slip flow. For a $P_i/P_o$ = 2.29, this difference is approximately +21% near the outlet. This is also visible in Figure 3(c) where different cross-sections along the y-direction show increase in streamwise velocity with a corresponding rise in wall velocity due to slip. As Kn increases due to lower density downstream, the slip effect increases. Figure 3(d) shows orders of magnitude difference between predicted slip and no-slip crosswise *v*- velocity component. However, it is significantly less in the magnitude ($10^{-6}$ m/s) as compared to streamwise *u*- velocity which is of the order of $10^{-1}$ m/s. This indicates that crosswise pressure difference is negligible.

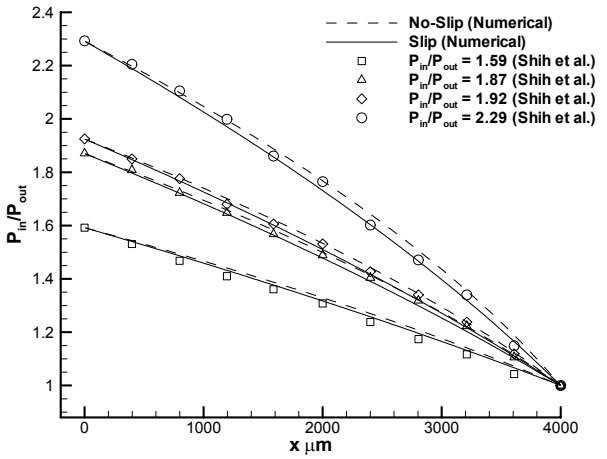


(a)

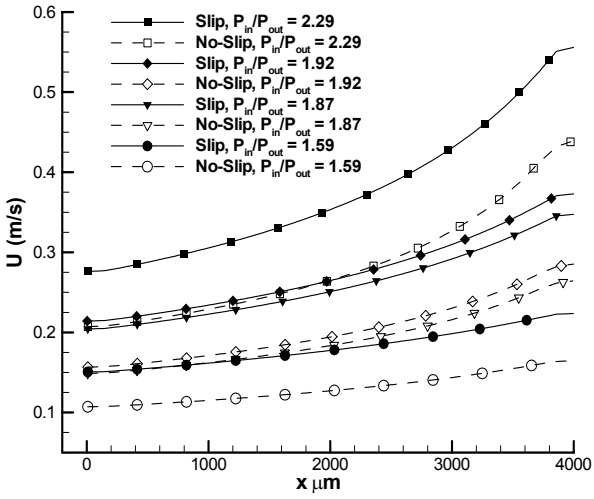


(b)

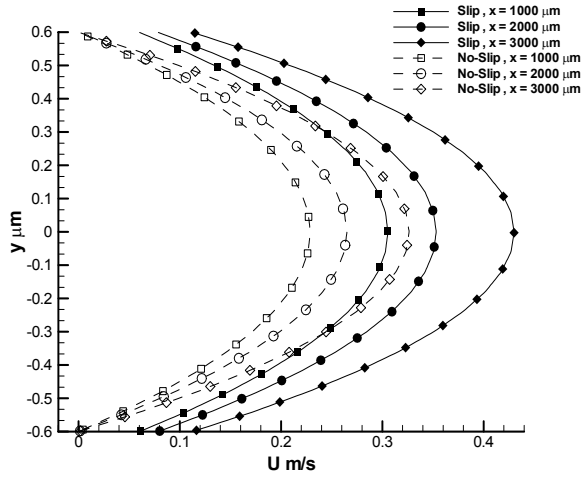


(c)

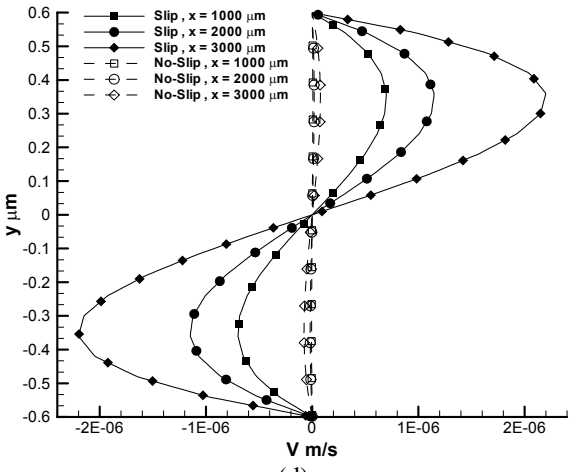


(d)

Figure 3. Comparison of (a) computed centerline pressure distribution with experimental data; (b) the centerline slip and no-slip velocity solutions; (c) slip and no-slip u-velocity and (d) v- velocity at three different cross-sections of the microchannel for $P_i/P_o$=2.29.

The only other experimental data available for this case is the mass flow rate, which has been compared with the slip and no-slip solutions in Figure 4. The experimental data from Shih *et al.* [3] is plotted with ±3% error bar validating the finite element results. The maximum mass flow rate is found to be ~ 6.82 x $10^{-12}$ kg/s for helium for the given pressure ratios. The slip flow comparison with the experimental data is within ~8%; whereas the no-slip solution is 28% lower.

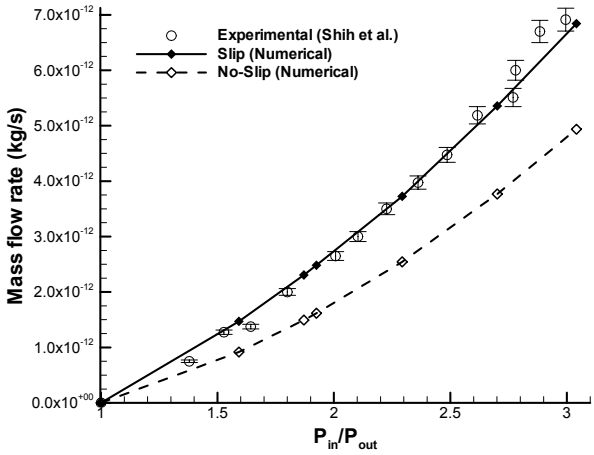


Figure 4. Computed mass flow rate (kg/s) comparison with experimental data of Shih *et al.*[3]

**Case II** is based on experimental[4,5] measurement of mass flow rates for Helium gas. The microchannel has an aspect ratio of 5639 having a length of 7500 μm and 1.33 μm height. It was manufactured using a two-wafer manufacturing process by etching an oxide grown on silicon. The outlet condition is atmospheric. Five different pressure ratios are used between 1.34 and 2.70 based on the outlet pressure yielding a maximum Knudsen number of 0.155 (transition regime) at the outlet. The computational geometry is same as for Case I consisting of 28×20 finite elements. Note that Chen *et al.*[6] utilized 6000×23 finite difference mesh to simulate this problem.

Figure 5 plots the slip and no-slip hydrodynamic solutions showing similar trend as of Case I for pressure and velocity. The maximum difference in slip and no-slip solutions is within 4% for pressure and nearly 24% for velocity, Figure 5(a)-(b). The small knee noticeable near the outlet for streamwise velocity solution is due to the imposed vanishing gradient boundary condition. The wall velocity at x = 5625 μm is approximately 50% more than that at x= 1875 μm, Figure 5(c). This also confirms the effect of slip with increasing Kn.

The mass flow rates for microchannel have been compared with both the experimental data[4] and numerical solution[6] in Figure 5(d). The slip flow differs by only ~+2.5% with numerical slip-solution and a maximum of +7% from the experimental data. The mass flow rate for the slip solution is ~35% higher than no-slip solution.

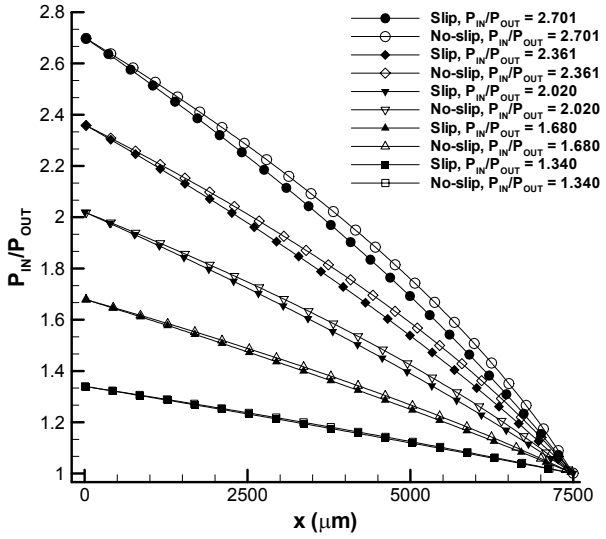


(a)

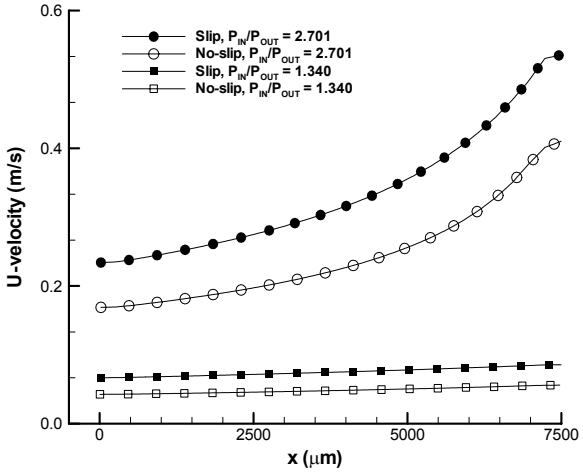


(b)

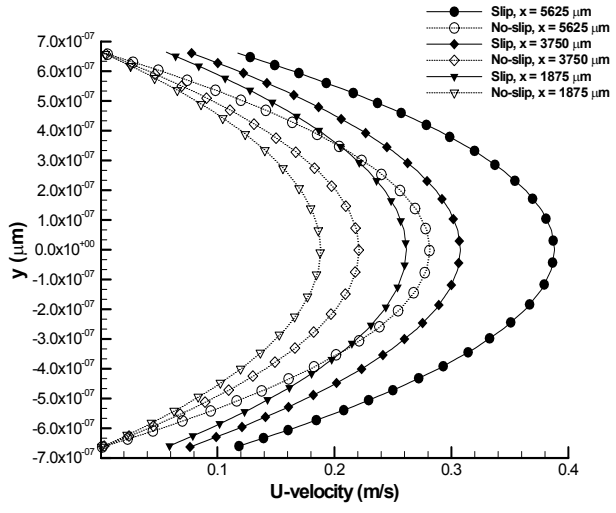


(c)

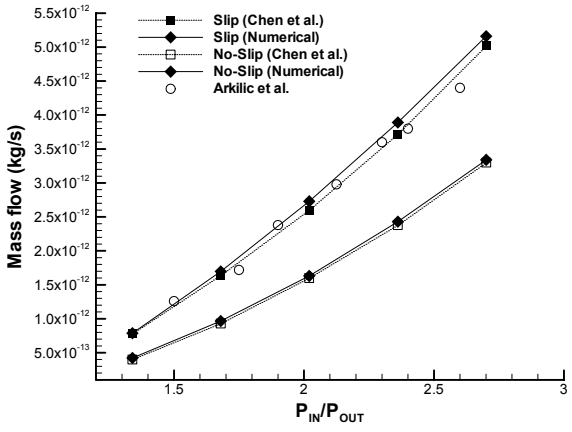


(d)

Figure 5. Comparison of (a) computed centerline slip & no-slip pressure distribution, (b) computed centerline slip and no-slip streamwise velocity; (c) u- velocity for slip and no-slip condition at three different cross-sections of the microchannel for *Pi/Po*=2.70; (d) computed mass flow rate (kg/s) compared with the experimental data of Arkilic *et al.*[4] and the numerical slip and no-slip mass flow rates from Chen *et al.*[6]

**Case III** for the given FMMR geometry is also modeled by using a 2337 node finite element mesh. The flow is simulated with aforementioned boundary conditions for two different temperatures: (1) Isothermal at 300K, and (2) chip wall temperature $T_w$ maintained at 600K. Figure 6 shows the flow structures for the isothermal case of 300 K. Figure 6(a) plots the particle trajectory in the symmetric half while the v-velocity contours are described in Figure 6(b). The peak is ~75 m/s near the slot exit region. Evidently, there is little flow in the plenum area. Velocity shoots up at the inlet region of the slot and stays high till the fluid expands at the very low pressure outlet.

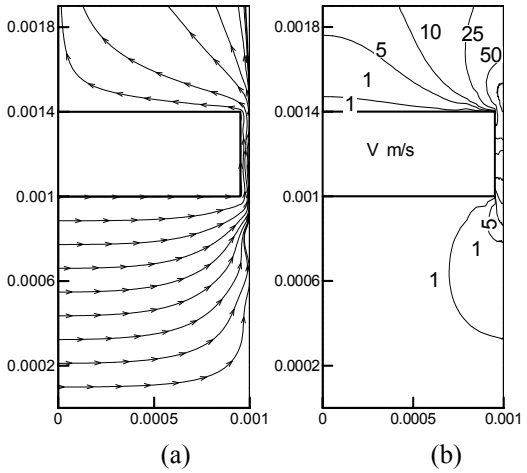


(a) (b)

Figure 6. Flow contours through the symmetric half of the FMMR slot with isothermal conditions at T = 300 K, $\sigma_V$ = $\sigma_T$ = 1.0, (a) particle trajectory, (b) v-velocity in m/s.

Next using this solution as initial condition, numerical simulation is run with the chip wall temperature fixed at 600K. This results in higher streamwise velocities as the propellant is excited with the injected power through the surface gas interaction. Figure 7(a) shows similar trajectory as of the isothermal case in Figure 6(a). However, the v-velocity component plotted in Figure 7(b) shows significant increase exceeding well over 100m/s. In Figure 7(c) a sharp drop in pressure occurs inside the slot while very little change is observed in the plenum or outside. The temperature contours in Figure 7(d) show that the fluid absorbs heat from the wall and the temperature of the fluid quickly becomes equal to that of the wall within the slot and the exit region.

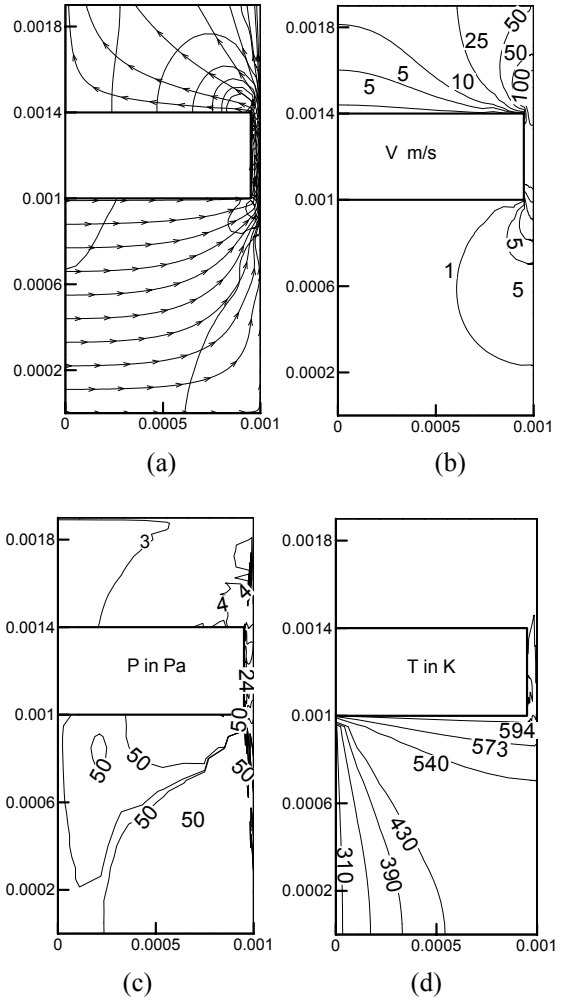


Figure 7. Flow contours through the symmetric half of FMMR with chip temperature fixed at T = 600 K, $\sigma_V = \sigma_T = 1.0$, (a) particle trajectory overlay on u-velocity contours, (b) v-velocity contours in m/s, (c) pressure in Pa, and (d) temperature in K.

The fluid thermal details inside the slot are shown in Figure 8. In Figure 8(a), the u-velocity component shows an anti-symmetric pattern as the argon gas comes in from and shoots out towards both sides horizontally near the slot inlet and exit plane, respectively. The magnitude of u-velocity remains small ($\sim 10^{-3}$ m/s). The streamwise component of velocity (v) in Figure 8(b), however, increases rapidly. The maximum v-velocity reaches upto 160 m/s at the slot exit. Interestingly, v-velocity slows down in the middle section of slot where the pressure remains stagnant along nearly 80% of the slot length (from 0.00004m to 0.00036m) as shown in Figure 8(c). This suggests a shorter length of the slot may be beneficial. The temperature contours plotted in Figure 8(d) shows negligible variation in the distribution of energy but for the slight drop near the inlet and exit region of slot.

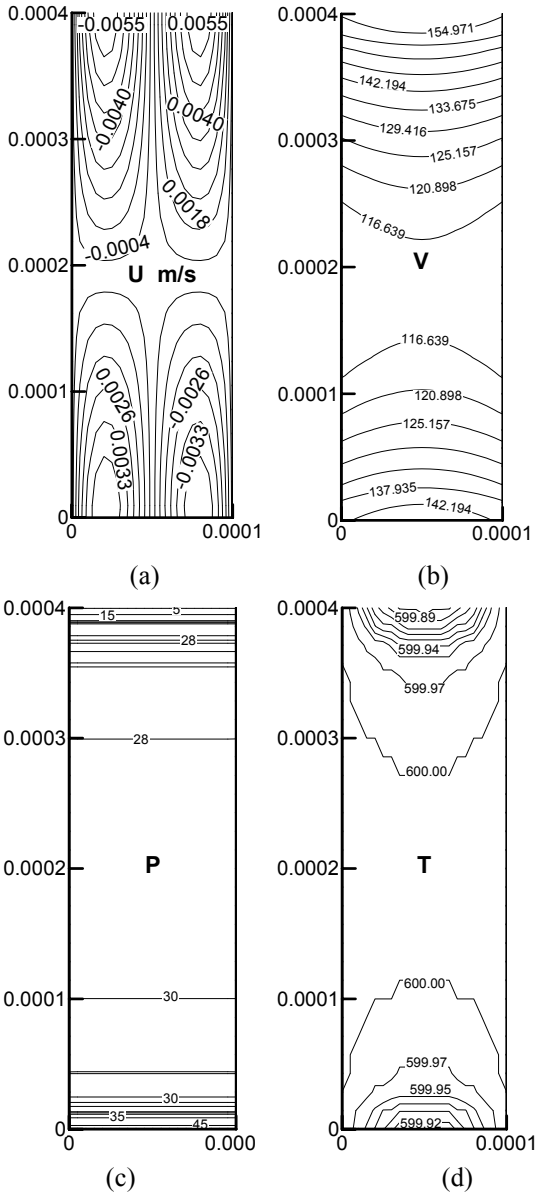


Figure 8. Zoomed in view of flow structures inside the slot at T = 600 K, (a) u-velocity in m/s, (b) v-velocity in m/s, (c) pressure in Pa, (d) temperature in K.

For the FMMR the thrust is generated due to the increase in energy of the propellant molecules in the expansion slots due to the gas-surface interactions. This thrust and specific impulse is calculated using the following equations,

$$\Im = \dot{m} v_{exit} = \int_{exit} \rho \mathbf{V} \left( \mathbf{V} \bullet d\mathbf{A}_s \right) \tag{4a}$$

$$I_{sp} = \frac{\Im}{\dot{m} g_0} = \frac{v_{exit}}{g_0} \tag{4b}$$

where $\dot{m}$ is the mass flow rate across the crossectional area $A_s$ of the slot, $v_{exit}$ is the average velocity at the exit of the slot and $g_0 = 9.80$ m/s$^2$ is the gravitational acceleration.

Table 3 shows the preliminary thrust calculations for the FMMR for two different temperature conditions. The wall temperature effect is found to be significant in increasing the thrust of the system. Note that for $\sigma_V = \sigma_T = 1.0$, the predicted mass flow rate (specific impulse) and thrust are at least one order and two orders of magnitude smaller, respectively, than that calculated by DSMC method.[17] For the same outlet density (pressure) and similar geometry, this means that the predicted gas velocity has to be at least an order of magnitude larger which will require adjustment of the wall accommodation coefficients. For $\sigma_V = 0.3$, $\sigma_T = 1.0$, the flow increases nearly 3.5 times, while for $\sigma_V = 0.1$, the massflow rate is $0.63\times10^{-6}$ kg/s and the specific impulse is 103.9 sec which are of the same order as of previous DSMC calculation.[17]

| Temp (K) | Wall Slip | $v_{exit}$ (m/sec) | Massflow (kg/sec) | Thrust ($\mu$N) | Specific Impulse (sec) |
|---|---|---|---|---|---|
| 300 | $\sigma_V$=1.0 | 75 | $8.96\times10^{-8}$ | 6.27 | 7.14 |
| 600 | $\sigma_T$=1.0 | 160 | $1.1\times10^{-7}$ | 17.6 | 16.33 |
| 600 | $\sigma_V$=0.3 $\sigma_T$=1.0 | 551 | $0.34\times10^{-6}$ | 188.1 | 54.73 |
| 600 | $\sigma_V$=0.1 $\sigma_T$=1.0 | 1018 | $0.63\times10^{-6}$ | 641.3 | 103.88 |

Table 3. Mass flow rate and thrust calculations for the FMMR.

## 6. CONCLUSIONS

A finite element based hydrodynamic model has been benchmarked using experimental and numerical data available in the literature. The gaseous flow through microchannel has been modeled using both no-slip and first order slip boundary conditions for Knudsen number ranging 0.155-0.17. For Case I and II the maximum deviation of the mass flow rate from the experimental data is only within −8% and +7% respectively while for Case II it is comparable within ~+2.5% of the reported numerical data on a very fine mesh. For the free-molecule FMMR case with exit Kn of 17.72, wall boundary conditions have significant effect on the solution prediction. With diffusive wall interaction, the fluid velocity increase from 75 m/s to 160 m/s as the power input through the chip surface goes from 300 K to 600 K. Consequently, the predicted thrust nearly triples from 6.2 μN to 17.6 μN. However, these predictions are significantly lower than that of the published DSMC results indicating specular nature of wall properties. As we decrease $\sigma_V$, the momentum accommodation coefficient, from 1 to 0.1, the flow increases by an order of magnitude validating the hydrodynamic prediction in free molecule regime. Our predicted mass flow rate, thrust and specific impulse are of the same order as predicted previously with DSMC method. We infer that the finite element based hydrodynamic model is suitable for exploratory flow studies through microstructures. The computed pressure distribution indicates a shorter slot design may improve microthruster efficiency. Future studies should be directed to affirm this conclusion.

## ACKNOWLEDGEMENTS

The first author's research was partially sponsored by NASA and AFRL grants. Authors acknowledge the support of NSF cooperative agreement ACI-9619020 through which the National Partnership for Advanced Computational Infrastructure at the San Diego Supercomputer Center provided the computing resources. Authors had many thoughtful discussions with Dr. Andrew Kestdever during the FMMR simulation process.

## REFERENCES

[1]Liu, J., Tai, Y.C., Pong, K. & Ho, C.M., 1993, "Micromachined channel/pressure sensor systems for micro flow studies," *7th International. Conference on Solid State Sensors and Actuators, Yokohoma*, *IEEEJpn,* pp.995-997.

[2]Pong, K. C., Ho, C., Liu, J., & Tai, Y., 1994, "Non-linear pressure distribution in uniform microchannels," *Application of Microfabrication to Fluid Mechanics,* FED – 197, pp. 51-56.

[3]Shih, J.C., Ho, C.M., Liu, J. & Tai, Y.C., 1996, "Monatomic and polyatomic gas flow through uniform microchannels," *ASME DSC* 59,pp. 197-203.

[4]Arkilic, E.B., Breuer, K.B. & Schimidt, M.A, 1994, "Gaseous Flow in Microchannel," *Application of Microfabrication to Fluid Mechanics, ASME,* FED- 197, pp. 57-66.

[5]Arkilic, E.B., Breuer, K.B. & Schimidt, M.A. 2001, "Mass flow and tangential momentum accommodation in

silicon micromachined channels," *Journal of Fluid Mechanics*, vol. 437,pp. 29-43.

[6]Chen, C. S., Lee, S. M., and Sheu, J.D. ,1998, "Numerical analysis of gas flow in microchannels," *Numerical Heat Transfer, Part A* 33,pp. 749-762.

[7]Maxwell, J.C., 1879, "On stresses in rarefied gases arising from inequalities of temperature," ***Philosophical Transactions of the Royal Society Part 1,*** vol.170, pp.231-56.

[8]Smoluchowski, von M., 1898, "Ueber wärmeleitung in verdünnten gasen", ***Annalen der Physik und Chemi,*** vol. 64, pp. 101-30.

[9]Karniadakis, G., and Beskok, A.,2002 "Micro Flows-Fundamentals and Simulation," *Springer-Verlag, New York.*

[10]Roy, S., Raju, R., Chuang, H., Kruden, B., and Meyyapan, M., 2003, "Modeling gas flow through microchannels and Nanopores," *Journal of Applied Physics,* vol. 93, n.8, pp. 4869-4878.

[11]Salomons, E., Mareschal M., 1992, Usefulness of the Burnett description of strong shock waves, *Physics Review Letters*, vol. 69, pp. 269–72.

[12]Bird, G.A., 1994, "Molecular Gas Dynamics and the Direct Simulation of Gas Flows," *Clarendon Press, Oxford, United Kingdom*.

[13]Cooper, S., Kruden, B., Meyyapan, M., Roy, S. and Raju, R., 2004, "Gas transport characteristics through a carbon nanotubule," *Nano Letters,* (web released on Dec 23, 2003).

[14]Raju, R. and Roy, S., 2004, "Hydrodynamic model for microscale flows in a channel with two 90° bends," *Journal of Fluids Engineering*, vol. 126, n. 3 (in press).

[15]Molho, J.I., Herr, A.E., Mosier, B.P., Santiago, J.G., Kenny, T.W., Brennen, R.A., Gordon, G.B., and Mohammadi, B. ,2003, "Optimization of turn geometries for microchip electrophoresis," *Analytical Chemistry,* vol. 73, pp. 1350-1360.

[16]Jahn, R., 1968, "Physics of Electric Propulsion," ***McGraw Hill, New York.***

[17]Ketsdever, A., Wadsworth, D. and Muntz , E.P., 2000, "Influence of gas-surface interaction models on Predicted performance of a Micro-resistojet," ***34th Thermophysics Conference,*** AIAA 2000-2430**.**

[18]Ketsdever, A.D., Green, A.A., Muntz, E.P., Wadsworth, D.C. and Vargo, S.E., 2000, "Heat Transfer measurements and calculations of a MEMS Fabricated Resistojet: Initial Results," ***34th AIAA Thermophysics Conference, Denver,*** AIAA 2000-2505**.**

[19]Ketsdever, A. , Wadsworth, D. and Muntz, E.P., 2001, "Predicted performance and systems analysis of the Free Molecule Micro-resistojet," ***Micropopulsion of Small Spacecraft, Progress in Astronautics and Aeronautics, 187, eds. M. Micci, M. and A. Ketsdever, AIAA, Reston, VA,*** Chapter 5**.**

[20]Wong, J., Ketsdever, A. and Reed, H., 2003, "Numerical modeling of the Free Molecule Micro-resistojet prototype and next generation designs evaluation," ***36th Thermophysics Conference,*** AIAA 2003-3581**.**

[21]Piekos, E. & Breuer, K., 1995, "DSMC modeling of microchannel devices," ***AIAA Thermophysics Conference, San Diego, CA,*** AIAA 95-2089.

[22]Baker, A.J., Iannelli, J., Chaffin, D.J. and Roy, S. 1998 "Some recent adventures into improved finite element CFD methods for convective transport," *Computer Methods in Applied Mechanics and Engineering,* vol. 151, pp. 27-42.